UNIVERSIDADE TECNOLÓGICA FEDERAL DO PARANÁ

GLÁUCIO PORCIDES CZEKAILO

SOBRE O USO DA DFT-S-OFDM GENERALIZADA PARA REDUZIR A INTERFERÊNCIA INTER-NUMEROLOGIA EM REDES 5G-NR

DISSERTAÇÃO

CURITIBA

2022

GLÁUCIO PORCIDES CZEKAILO

SOBRE O USO DA DFT-S-OFDM GENERALIZADA PARA REDUZIR A INTERFERÊNCIA INTER-NUMEROLOGIA EM REDES 5G-NR

On the Use of Generalized DFT-s-OFDM to Reduce Inter-Numerology Interference in 5G-NR Networks

Dissertação apresentada como requisito para obtenção do título(grau) de Mestre em Engenharia Elétrica e Informática Industrial, do Programa de Pós-Graduação em Engenharia Elétrica e Informática Industrial, da Universidade Tecnológica Federal do Paraná (UTFPR).

Orientador: Prof. Dr. Bruno Sens Chang
Coorientador: Prof. Dr. Glauber Gomes de Oliveira Brante

CURITIBA

2022

Ministério da Educação
Universidade Tecnológica Federal do Paraná
Campus Curitiba

GLAUCIO PORCIDES CZEKAILO

SOBRE O USO DA DFT-S-OFDM GENERALIZADA PARA REDUZIR A INTERFERÊNCIA INTER-NUMEROLOGIA EM REDES 5G-NR

Trabalho de pesquisa de mestrado apresentado como requisito para obtenção do título de Mestre Em Ciências da Universidade Tecnológica Federal do Paraná (UTFPR). Área de concentração: Telecomunicações E Redes.

Data de aprovação: 04 de Julho de 2022

Dr. Bruno Sens Chang, Doutorado - Universidade Tecnológica Federal do Paraná

Dr. Carlos Aurelio Faria Da Rocha, Doutorado - Universidade Federal de Santa Catarina (Ufsc)

Dr. Joao Luiz Rebelatto, Doutorado - Universidade Tecnológica Federal do Paraná

Dedico este trabalho à minha família.

ACKNOWLEDGEMENTS

A Deus, pela vida, e por ser o amigo em quem encontrei força durante a elaboração desse trabalho.

A minha esposa, Gabriele Maurício Czekailo, por abrir mão de próprios anseios para me ajudar neste tempo.

Aos meu pais, por acreditarem em mim e serem meus maiores incentivadores.

Ao meu orientador, Bruno Sens Chang, que me mostrou caminhos, inspirou ideias, e me ajudou com maestria.

Ao meu coorientador, Glauber Brante, pelas pertinentes análises e contribuições para o desenvolvimento deste trabalho.

Ao meu amigo e gestor, Thiago Henrique dos Santos Picharski, seu apoio foi fundamental e me deu oportunidade de ser bem sucedido nos meus estudos. Minha sincera gratidão.

A professores e colegas, que ajudaram de forma direta e indireta na conclusão deste trabalho.

You can't go back and change the beginning,
but you can start where you are and change the
ending. (LEWIS, C.S.)

RESUMO

CZEKAILO, Gláucio. **Sobre o uso da DFT-s-OFDM Generalizada para reduzir a Interferência Inter-Numerologia em redes 5G-NR**. 2022. 48 f. Dissertação (Mestrado em Engenharia Elétrica e Informática Industrial) – Universidade Tecnológica Federal do Paraná. Curitiba, 2022.

Os sistemas de multiplexação por divisão de frequências ortogonais, ou OFDM, com prefixo cíclico (CP-OFDM) são a forma de onda base nas redes móveis de quinta geração (5G-NR), com a versão pré-codificada da Transformada Discreta de Fourier (DFT-s-OFDM) como uma alternativa em cenários limitados pela razão potência de pico e potência média, ou PAPR. No entanto, como as redes 5G-NR utilizam múltiplas numerologias, a coexistência destas introduz uma nova não ortogonalidade ao sistema, conhecida como Inteferência Inter-Numerologia (INI). O presente trabalho propõe uma alternativa ao uso do prefixo cíclico por meio da forma de onda DFT-s-OFDM Generalizada (G-DFT-s-OFDM). Nossos resultados mostram que o uso da forma de onda G-DFT-s-OFDM reduz significativamente o INI nas redes 5G-NR.

Palavras-chave: Redes 5G-NR. Interferência Inter-Numerologia. DFT-s-OFDM Generalizada.

ABSTRACT

CZEKAILO, Gláucio. **On the Use of Generalized DFT-s-OFDM to Reduce Inter-Numerology Interference in 5G-NR Networks**. 2022. 48 p. Dissertation (Master's Degree in Electrical and Computer Engineering) – Federal University of Technology - Paraná. Curitiba, 2022.

Orthogonal Frequency Division Multiplexing (OFDM) systems with a Cyclic Prefix (CP-OFDM) are the base waveform in fifth-generation New Radio (5G-NR) mobile networks, with the Discrete Fourier Transform precoded version (DFT-s-OFDM) as an alternative in Peak-to-Average Ratio (PAPR) limited scenarios. However, since 5G-NR networks use multiple numerologies, the coexistence of these numerologies introduces a novel non-orthogonality in the system, known as Inter-Numerology Interference (INI). The present work proposes an alternative to the use of the CP by means of the Generalized-Discrete Fourier Transform-spread-Orthogonal Frequency Division Multiplexing (G-DFT-s-OFDM) waveform. Our results show that the use of the G-DFT-s-OFDM waveform significantly reduces the INI in 5G-NR networks.

Keywords: 5G-NR networks. Inter-Numerology Interference. Generalized DFT-s-OFDM.

LIST OF FIGURES

LIST OF TABLES

LIST OF ACRONYMS

INITIALISM

3GPP	3rd Generation Partnership Project
CNPq	Conselho Nacional de Desenvolvimento Científico e Tecnológico
GSA	Global mobile suppliers' Associations
IMT	International Mobile Telecommunications
ITU	International Telecommunications Union

ACRONYMS

5G-NR	Fifth Generation New Radio
AI	Artificial Intelligence
AVs	Autonomous Vehicles
BPSK	Binary Phase Shift Keying
CP	Cyclic Prefix
DFT-s-OFDM	Discrete Fourier Transform - spread - OFDM
GFDM	Generalized Frequency Division Multiplexing
IDFT	Inverse Discrete Fourier Transform
IFFT	Inverse Fast Fourier Transform
INI	Inter Numerology Interference
ISI	Inter-Symbolic Interference
IoT	Internet of Things
LTE	Long Term Evolution
MCM	Multicarrier Modulation
NFV	Network Function Virtualization
NSCS	Narrow Subcarrier Spacing
OFDM	Orthogonal Frequency Division Multiplexing
OOB	out-of-band
PAPR	Peak to Average Power Ratio
RB	Resource Block
SCS	Subcarrier Spacing
SDN	Software-Defined Networking
SNR	Signal-to-Noise Ratio
UFMC	Universal Filtered MultiCarrier
URLLC	Ultra-Reliable Low Latency Communications
UW	Unique Word
VR	Virtual Reality
WSCS	Wide Subcarrier Spacing

ZT	Zero-Tail
eMBB	Enhanced Mobile Broadband
mMTC	Massive Machine-Type Communications

LIST OF SYMBOLS

LATIN LETTERS

T	Period	$[\mathrm{s}]$
Q	WSCS/NSCS SCS ratio	

GREEK LETTERS

μ	Numerology index
η	Indexes allocation ratio
δ	Head and Tail multiplier

SUMÁRIO

1 INTRODUCTION

The 3GPP in its Release 15 defined the complete structure for the physical layer of 5G-NR and its structural differences with respect to LTE ((3GPP), 2018b; (3GPP), 2018a). Their biggest difference applies to the physical layer, which is now designed to support multiple configurations by multiplexing different numerologies. The reason for this change is due to the use-case scenarios of 5G-NR: enhanced Mobile BroadBand (eMBB), massive Machine-Type Communications (mMTC) and Ultra-Reliable Low Latency Communications (URLLC).

OFDM is a transmission technique that divides the available bandwidth into multiple subcarriers. In addition, the usage of a CP in OFDM-based systems allows the use of simple (inverse) Fast Fourier Transforms ((I)FFTs), which reduces the complexity of the transceiver and equalization processes. Due to these factors, CP-OFDM has been used as a basic waveform in various radio technologies such as LTE, IEEE 802.11, and recently in 5G-NR.

A *numerology* defines parameters such as the allocated subcarrier spacing, OFDM symbol duration, CP duration, and slot duration for data channels (DEMMER *et al.*, 2018). In 5G-NR, a total of five numerologies are provided, with the conventional LTE numerology chosen as the base one. The base numerology considers a subcarrier spacing $\Delta_f = 15$ kHz, while the other numerologies are 2^μ multiples of Δ_f, with μ corresponding to the numerology index. These multiple numerologies provide flexibility, adapting each usage scenario to its demands in terms of bandwidth, robustness, *etc*.

However, the combination of CP-OFDM with multiple numerologies operating simultaneously results in a new type of interference, denoted as INI. That happens due to the loss of orthogonality between subcarriers of different numerologies in the frequency domain, as well as the difficulty in achieving symbol alignment in the time domain. At the same sampling rate, the FFT window of an OFDM symbol from one numerology does not align with the one from another numerology, making synchronization within the frame difficult. DFT-s-OFDM schemes have been proposed in order to improve performance in Peak-to-Average Ratio (PAPR)-limited scenarios in 5G-NR (MYUNG *et al.*, 2006). Nevertheless, it has the same limitations of CP-OFDM regarding the INI, since a CP is also employed and the OOB emissions are the same. Therefore, new strategies to reduce INI are welcome, and have been studied by the recent literature.

In this work, we present an alternative to DFT-s-OFDM in multi-numerology 5G-NR systems. Our proposal considers a generalized DFT-s-OFDM (G-DFT-s-OFDM) system (BERARDINELLI *et al.*, 2016; BERARDINELLI, 2017), which has better time and frequency localization when compared to the regular one, while being less complex than filtered systems such as the GFDM, UFMC and Filter Bank Based Multicarrier (FBMC) (BERARDINELLI, 2017). This work presents simulations of G-DFT-s-OFDM operating in different scenarios, as well as a comparison with the conventional OFDM systems with a CP. Our results show that the use of G-DFT-s-OFDM is a valid and easy-to-implement alternative in multi-numerology 5G-NR, exhibiting much smaller INI values when compared to CP-OFDM. For instance, we show that it is possible to reduce the peak INI by at least 20 dB by using the G-DFT-s-OFDM. Moreover, the guard bands needed for a INI of -40 dB are at least 3.5 times smaller with respect to CP-OFDM systems. Finally, another important advantage is that G-DFT-s-OFDM maintains system compatibility, and it can actually be used along with DFT-s-OFDM/CP-OFDM if needed.

1.1 AIM AND OBJECTIVES

1.1.1 Aim

Evaluate the usability of G-DFT-s-OFDM system in terms of INI performance for 5G-NR networks.

1.1.2 Objectives

- Model the G-DFT-s-OFDM transmission and receiver scheme for 5G, clarifying the difference with respect to the 5G-NR standard.
- Propose a solution based on G-DFT-s-OFDM scheme to mitigate the INI.
- Simulate the proposed scheme to generate INI results from G-DFT-s-OFDM and CP-OFDM systems.
- Analyze the INI simulation results for different scenarios and their impact in the system performance.

1.2 DOCUMENT STRUCTURE

The rest of this document is organized as follows. Session II presents the literature review, covering a brief introduction to 5G-NR networks, CP-OFDM, DFT-s-OFDM and G-DFT-s-OFDM systems. Session III exposes the methods used to achieve the objectives of the work - the considered system model is presented in this Section. In Section IV the simulation results taking into account the aforementioned system model are shown and discussed. Finally, Section V presents the concluding remarks and some perspectives regarding future work.

1.3 SUBMITTED ARTICLE

The following article was submitted during the development of this work:

- G. P. Czekailo, B. S. Chang and G. Brante, "On the Use of Generalized DFT-s-OFDM to Reduce Inter-Numerology Interference in 5G-NR Networks- submitted to XL Simpósio Brasileiro de Telecomunicações E Processamento de Sinais - SBrT 2022

2 LITERATURE REVIEW

2.1 5G-NR

Currently, the most popular mobile network type is LTE, being used by 5.8 billion users - 62% of the total users - according to the March 2021 report by the GSA (GSA, 2021). However, the constant evolution of mobile technologies - such as IoT, AI, VR, AVs - demands a new level of data rate, latency and power consumption. 5G-NR was designed to obtain a thousand-fold increase in data volume and the number of connected devices per area, a 100-fold improvement in user data rates, power consumption by a factor of 10 and decrease in latency by a factor of 5 with respect to LTE (ASSOCIATION *et al.*, 2015). The Cisco annual report published in February 2020 forecasts that by 2023, 5G-NR will support 10 percent of mobile connections with an average speed of 575 megabits per second, and also approximately 14.7 billion machine to machine type communication links (OKOGBAA *et al.*, 2022).

5G-NR networks were designed to have a better performance in terms of speed, reliability, and latency when compared with their predecessors. The main differences in its architecture are the service area divided into small geographical areas (called cells) and the multi-numerologies combination for the antennas. This modification optimizes the communication channel due to the device being connected to a local antenna in its cell - allowing higher frequencies, and their data being exchanged using the numerology which has the best performance for the channel characteristics (IBRAHIM *et al.*, 2022).

Nevertheless, 5G-NR keeps the OFDM waveform already used in LTE. The main difference in this aspect is that 5G-NR supports multiple numerologies. As stated before, a numerology defines parameters such as the allocated subcarrier spacing, OFDM symbol duration, CP duration, and slot duration for data channels (DEMMER *et al.*, 2018). Therefore, numerologies can be used to meet the demands of each service class of 5G. For example, numerologies with a small SCS are more suitable for mMTC, since they can support higher number of simultaneously connected devices within the same bandwidth and require lower power. Numerologies which have an intermediate SCS are appropriate for eMBB, since it requires high data rate and significant bandwidth. Lastly, numerologies with a long SCS are more suitable for delay-sensitive applications, an example of usage are transmissions which use the URLLC service due to their shorter symbol duration. Note that the numerologies selection does not depend just on the service to be supported, but factors such as cell size, time variation of the channel, delay spread, etc., also need to be taken into account when choosing a numerology (KIHERO *et al.*, 2019).

Table 1 – 5G-NR Numerologies

μ	Δ_f (kHz)	RB (kHz)	T_{OFDM} (μs)	T_{CP} (μs)
0	15	180	66.67	4.69
1	30	360	33.33	2.34
2	60	720	16.67	4.17|1.17
3	120	1440	8.33	0.58
4	240	2880	4.17	0.29

Source: Adapted from (KIHERO *et al.*, 2019)

Table 1 summarizes the parameters adopted by the 5 different numerologies of 5G-NR. A total of five numerology options are provided with the conventional LTE numerology ($\mu = 0$) chosen as the base numerology. A numerology μ is defined mainly by its subcarrier spacing Δ_f (in kHz), which in turn defines the bandwidth occupied by the RB. The RB in 5G defines the smallest contiguous transmission bandwidth that can be used, which is constructed by combining 12 subcarriers. Then, for a given subcarrier spacing Δ_f, the numerology defines an OFDM symbol period T_{OFDM} and a CP period T_{CP}, both in μs.

Figure 1 – 5G service classes.

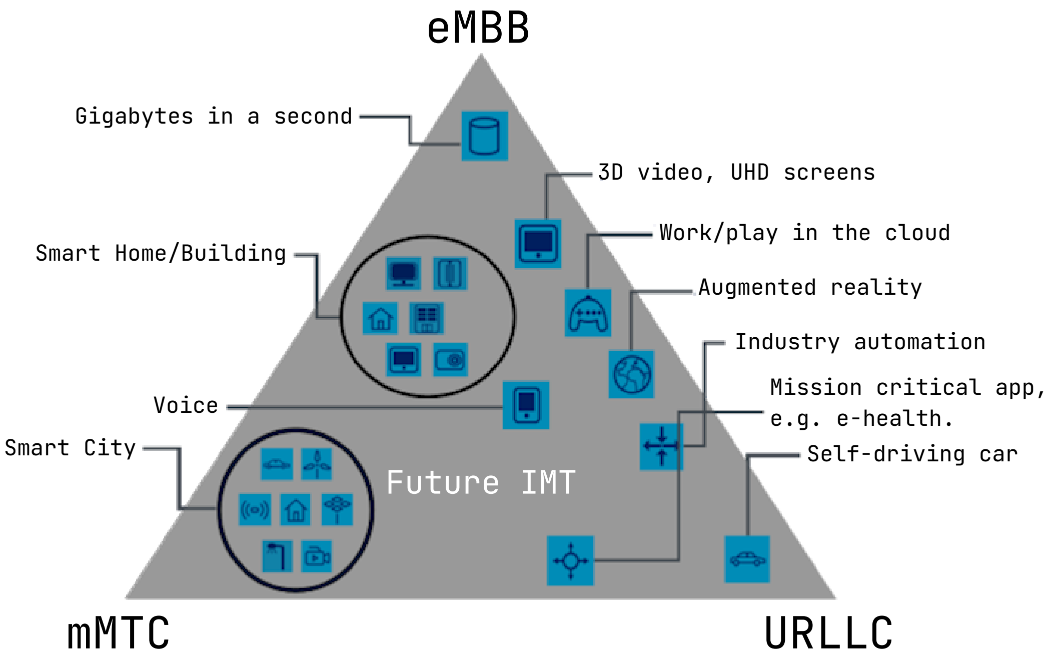

Source: Adapted from (ANDREEV, 2017)

Figure 1 shows how emerged technologies are placed into 5G-NR services. The IMT in the image means International Mobile Telecommunications, which is a standard and set of specifications for 5G networks established by the ITU. Therefore, the image gives a context about how the service classes are being used, and helps to understand how 5G-NR contributes to their implementation. In addition, an explanation about each service can be found in the following paragraphs.

mMTC, as the name suggests, deals with massive access by a large number of devices - for example, providing wireless connectivity to a huge number of often low-complexity low-power machine-type devices. Therefore, unlike other Machine-type Communications methods, where peak rates, availability, latency and reliability are prioritized, the main goal of this system is flexible connectivity for an increasing number of devices, wide area coverage and deep indoor penetration. A typical example of mMTC is the collection of the measurements from a massive number of sensors, such as smart metering (BOCKELMANN *et al.*, 2016).

The traffic of mobile broadband is ever growing, which requires increased coverage and efficiency of mobile networks. In addition, emerging technologies arise (e.g. Virtual Reality, Augmented Reality, 4K/8K video), stimulated by the use of smartphones, software and services. So, eMBB communications consists in a set of methods which intend to fulfill the requirement of high throughput. Basically, these methods are related with the use of specific implementation in order to enhance the data rate, such as eMBB based Antenna Techniques, eMBB based Diversity Techniques, eMBB based Channel Techniques and eMBB based Coding and Modulation Techniques (ABDULLAH; AMEEN, 2021).

Finally, URLLC is a communication service for successfully delivering packets with stringent requirements, particularly in terms of availability, latency, and reliability. URLLC plays an essential role in providing connectivity for new services and applications from a vertical domain, which means a particular industry or group of enterprises in which similar products or services are developed, produced, and provided. Examples of vertical domains are factory automation, autonomous driving and so on. So, URLLC enables support for emerging applications and services, such as wireless control and automation in industrial factory environments, inter-vehicular communications for improved safety and efficiency, and the tactile internet (LI *et al.*, 2018).

In addition to these services, in the latest releases of the 3GPP (16 and 17) the Network Slicing concept was highlighted, which belongs to the category of virtualization networking paradigm, together with Software-Defined Networking (SDN) and Network Function Virtualization (NFV). Network slicing can take advantage of SDN and NFV, but it can be seen as an independent technology. It enables the flexible and efficient creation of specialized end-to-end logical networks on top of shared network infrastructure. These logical networks are by themselves capable to supply a specific type of services, leading to benefits to industries that has particular occupation areas (e.g. vehicular, health services) (OLIMID; NENCIONI, 2020).

All those services and requirements ask for a flexible network in terms of waveform, numerology and frame structure. The 5G network has in its construction the possibility to cover that demand; however, new complications arise due to the flexibility added. The main one related with this work is the Interference-Numerology Interference, caused by the orthogonality loss between OFDM symbols with different duration and subcarrier spacings (KIHERO *et al.*, 2019).

2.2 OFDM

The Orthogonal Frequency Division Multiplexing (OFDM) system is a special case of MCM, which is a transmission principle that splits the transmitter data into several parallel bit streams and modulates them into individual carriers or subcarriers (WEINSTEIN, 2009). OFDM has orthogonal subcarrier spectrums, which allows their spectrum to overlap without restriction. This feature is realized with the IFFT and the Fast Fourier Transform to perform data modulation and demodulation.

Figure 2 – OFDM basic scheme.

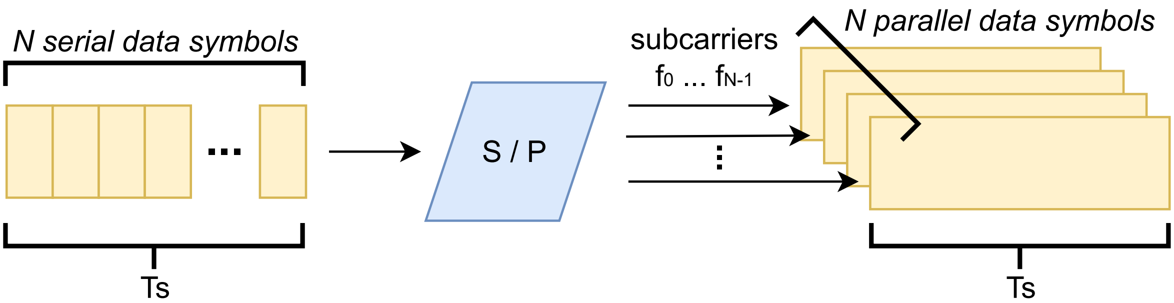

Source: Adapted from (WEISS; JONDRAL, 2004)

Figure 2 shows N data symbols being transmitted in the same period T_s of N parallel symbols due to the parallelism of low rate subcarriers. Therefore, the transfer rate experienced by both sides is the same, but with greater resistance to multipath interference.

To combat ISI the concept of the cyclic prefix was introduced. This cyclic extension of the OFDM symbol is used to simulate a circular convolution channel as long as the CP is longer than the channel impulse response length. Figure 3 shows the entire CP-OFDM transmitter scheme. However, a SNR penalty shows up with the loss of signal energy proportional to the length of the CP (TERRY; HEISKALA, 2002).

Figure 3 – CP-OFDM transmitter scheme.

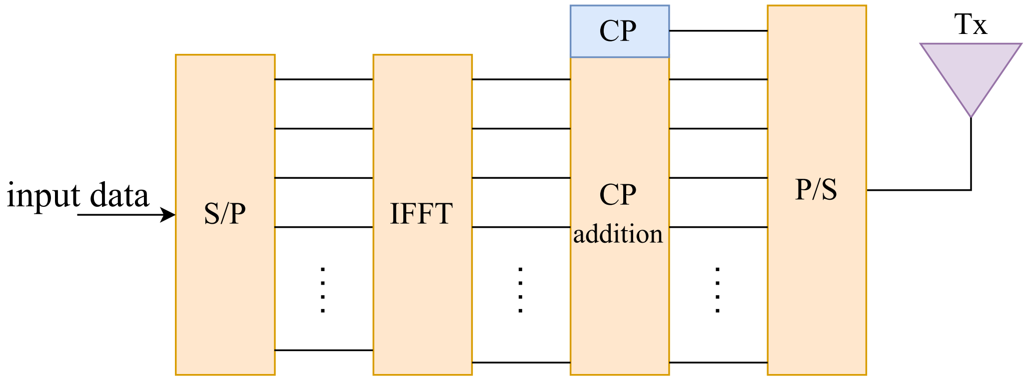

Source: Adapted from (MAKNI *et al.*, 2015)

One of the main problems faced by the OFDM technique is the PAPR inherent to its implementation (WULICH, 2005). As the transmitted signal is equal in the time domain to the sum of several narrow band signals, it has a high variation in value. This implies in lower power efficiency, requiring an improved power amplifier, one of the most expensive components of a radio system. Some techniques for peak cancellation (such as filtering, clipping and signal mapping) can be applied to diminish the PAPR, such as (JAWHAR *et al.*, 2019; WUNDER *et al.*, 2013; KIM *et al.*, 2017). However, they all add complexity to the system. Moreover, OFDM has high out-of-band emissions due to its use of the rectangular window (inherent to the FFT) to filter the subcarriers.

2.3 DFT-S-OFDM

Discrete Fourier Transform spread OFDM (DFT-s-OFDM) (MYUNG *et al.*, 2006) is a technique used in current mobile networks, such as 4G and 5G-NR, in low energy consumption scenarios such as the uplink. The only one difference with respect to regular OFDM systems is the spreading of the transmitted data symbols by a DFT. Therefore, each subcarrier carries a part of each modulated symbol.

Figure 4 – DFT-s-OFDM block diagram.

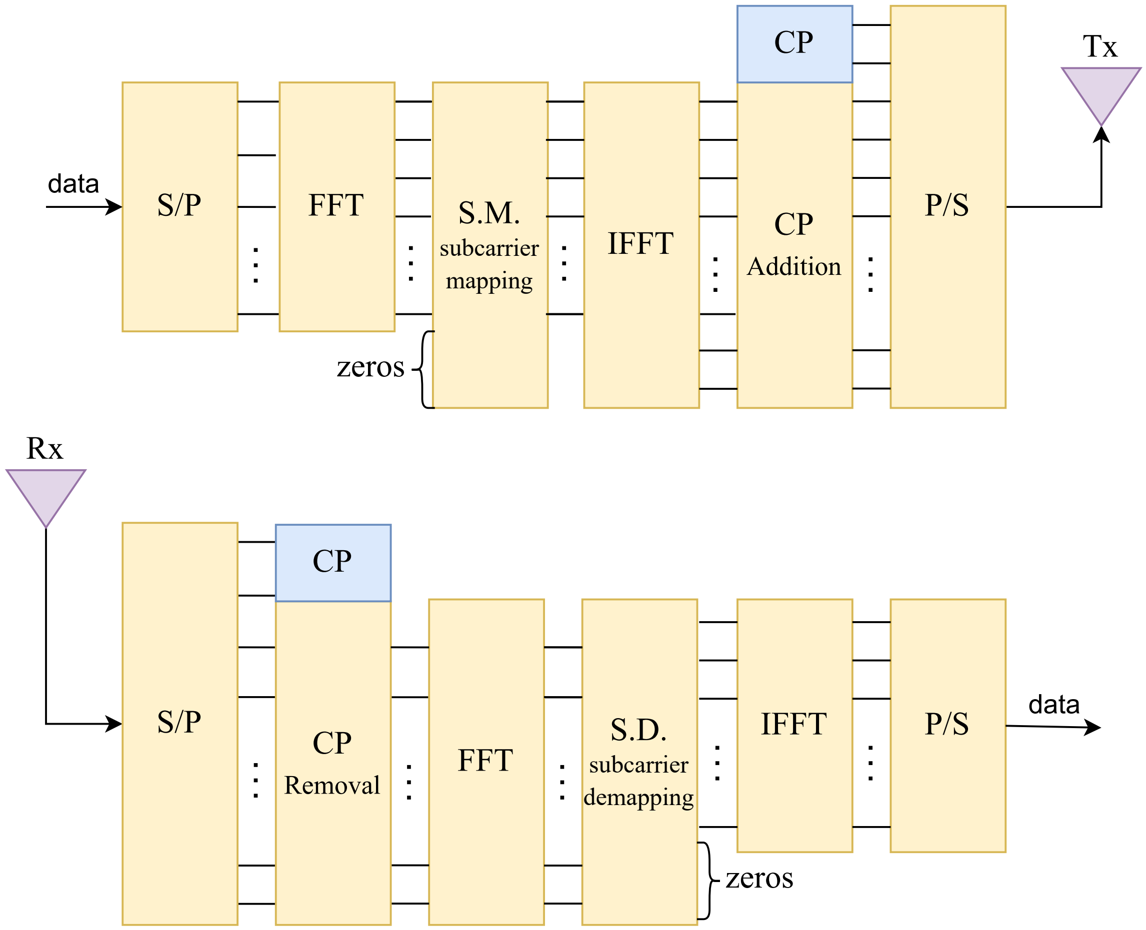

Source: Adapted from (BERARDINELLI, 2017)

Figure 4 presents a block diagram of both DFT-s-OFDM transmitter and receiver. For the transmitter, the first block is the serial/parallel (S/P) conversion block, which is responsible for converting the input data from serial to parallel, which is used in the next block. The second block is the FFT block, which transforms the input data to the frequency domain. The third block is the subcarrier mapping block, which maps the frequency domain data according to the determined (e.g., localized or distributed) mapping rule. This mapped sequence is used as input of an IFFT block. Then the CP is added to the signal in the next block.The sixth (and latest) transmitter block is a parallel/serial block, which is responsible for converting the modulated data from parallel to serial, making it possible to transmit the stream. For the receiver, the S/P and P/S blocks are at the same place and have similar functions - basically, they are used to prepare and organize the data for processing. The other four core blocks (CP removal / IFFT / subcarrier demapping / FFT) are inverted with respect to the transmitter and this combination is used to revert the operations made by the transmitter scheme, allowing the receiver to obtain the estimated data.

The major benefit of using DFT-s-OFDM is the reduced peak-to-average power ratio (PAPR) with respect to regular CP-OFDM, since DFT-s-OFDM is closer to a single-carrier waveform due to the spreading in the transmitter. Thus, its PAPR is largely influenced by the signal constellation used (KAKKAVAS *et al.*, 2017).Nevertheless, the OOB emissions of DFT-s-OFDM are the same ones from CP-OFDM, since the subcarrier formatting window is still the same.

2.4 INTER-NUMEROLOGY INTERFERENCE

The concept of multiple numerologies was designed to meet the needs of 5G-NR networks. This is due to the flexibility required in 5G applications, given the different requirements of eMBB, mMTC and URLLC scenarios. 5G-NR network numerologies are defined by ((3GPP), 2018b), which establishes the structure for their data channels.

Figure 5 – Inter-Numerology Interference in OFDM systems.

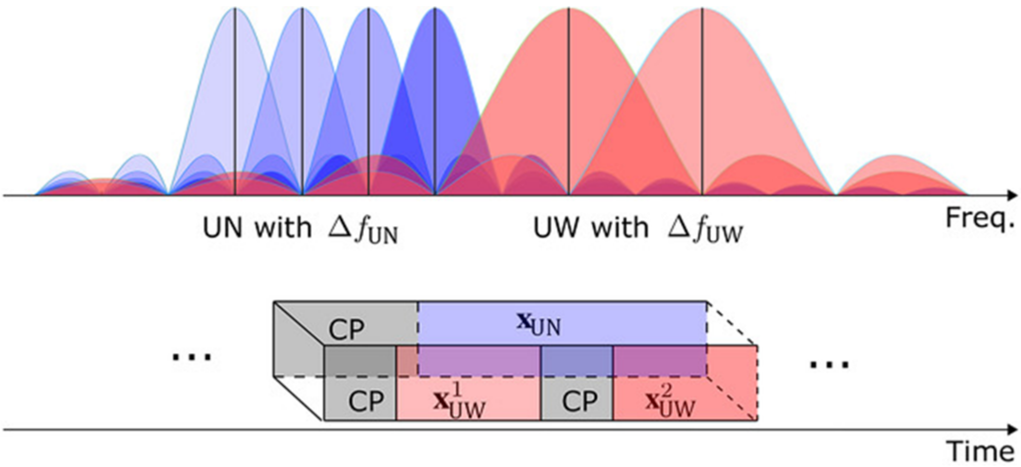

Source: (DOGAN-TUSHA *et al.*, 2021)

5G-NR networks are more flexible when compared to LTE because transmitters can operate simultaneously in more than one numerology. However, INI is one of the most important drawbacks of such simultaneous numerology usage. As shown in Figure 5, the INI is caused by the loss of orthogonality between OFDM symbols, given that they now have different durations and subcarrier spacings. Such orthogonality loss occurs because of the CP that has a different size for each numerology and it is added to each transmitted OFDM symbol. As an example, let us consider that symbols from two different numerologies, denoted by μ_1 and μ_2, are transmitted simultaneously. Let us also denote the symbol from numerology μ_1 as NSCS, while the symbol from numerology μ_2 is the WSCS. If the ratio of their subcarrier spacings is, *e.g.*, $Q = \Delta_{\mu_2}/\Delta_{\mu_1} = 2$, then there will be one OFDM NSCS symbol being transmitted at the same time of two OFDM WSCS symbols. In addition, the CP causes a misalignment of the symbol position with respect to the FFT window, breaking the orthogonality among the multiple numerologies.

Moreover, transmitters using different subcarrier spacings will have different spectral sidelobe lengths. Nevertheless, it is known that OFDM sidelobes have high OOB emissions, which will require a large guard band between transmissions in order to reduce the INI to an acceptable level, without resorting to filtering or other transmission strategies. This also becomes an issue in mMTC scenarios, where transmissions are sporadic and may not be fully synchronized.

2.5 GENERALIZED DFT-S-OFDM

The Generalized DFT-s-OFDM structure (BERARDINELLI *et al.*, 2016; BERARDINELLI, 2017) is based on the unification of two DFT-s-OFDM waveform variants without CP, which are: ZT DFT-s-OFDM, which places the data between low power sequences, which serve as a guard band; and UW DFT-s-OFDM, which positions the data between known sequences - for example, Zadoff-Chu sequences (BEYME; LEUNG, 2009). Note that in both cases (ZT DFT-s-OFDM and UW DFT-s-OFDM), the guard period shares with the data the number of DFT samples; therefore, the longer this period the less data will be transmitted, unlike the use of the CP, which is in addition of a fixed number of subcarriers per symbol. This same property means that in G-DFT-s-OFDM there is no break in the orthogonality of FFTs, differing from systems that use CP, such as CP-OFDM and DFT-s-OFDM.

The usage of G-DFT-s-OFDM brings several benefits to 5G-NR networks, primarily with respect to the INI. We recall that this interference is mainly caused by the loss of orthogonality between two OFDM symbols with different numerologies. G-DFT-s-OFDM replaces the CP by a head and tail, which share the subcarriers used by the transmitted data (BERARDINELLI, 2017). Thus, it is possible to generate the transmitted signal without losing the orthogonality among the numerologies. Another noteworthy benefit is the PAPR reduction, since the G-DFT-s-OFDM system inherits the low PAPR characteristic of DFT-s-OFDM. Finally, there is a significant reduction in OOB emissions when compared with CP-OFDM or DFT-s-OFDM systems (BERARDINELLI *et al.*, 2016), because G-DFT-s-OFDM has a known head and tail sequence, yielding a smooth transition between adjacent time symbols.

Figure 6 – G-DFT-s-OFDM scheme.

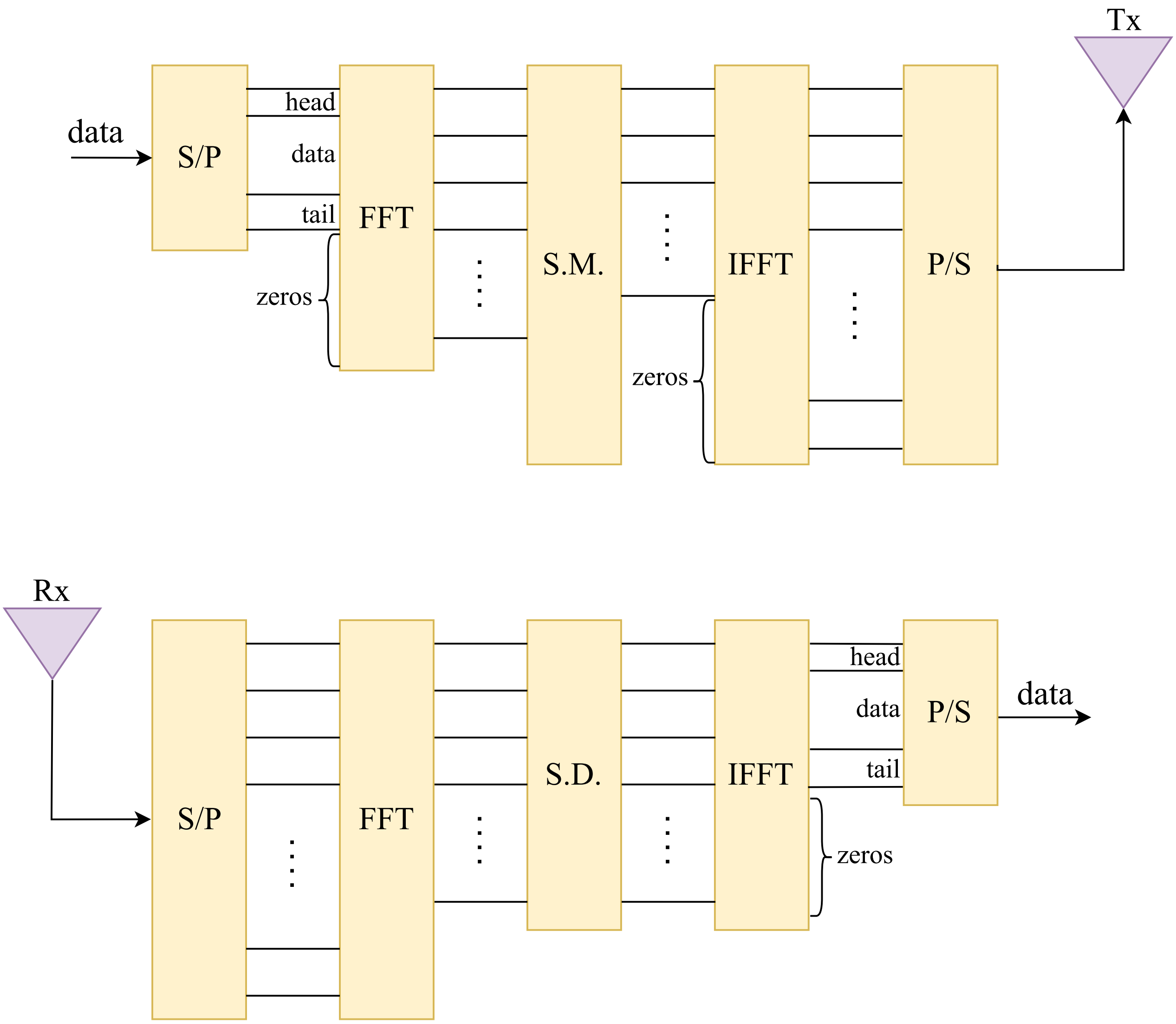

Source: Own authorship.

Figure 6 shows the G-DFT-s-OFDM transmitter and receiver. For the transmitter, the guard head/tail can be defined as either with almost zero power, denoted by Zero-Tail (ZT) DFT-s-OFDM, or by containing a known sequence, denoted by Unique Word (UW) DFT-s-OFDM. Note also that, in both cases, increasing the head/tail period decreases the amount of data to be transmitted. So, as expected, there is a tradeoff related with data and head/tail sizes. Anyway, in real world scenarios the decreased data rate is not so impacted since the head and tail used are relatively small (e.g. using 16/80 head/tail size for $N = 2048$, assuming 575 Mbps for CP-OFDM, the G-DFT-s-OFDM would have approximately 550 Mbps or a 4,6875$\%$ slower data rate). This is different from CP-OFDM, which has a fixed number of data subcarriers per symbol. Indeed, this property is responsible for maintaining the orthogonality of the FFTs in

G-DFT-s-OFDM.

The transmitted signal in a G-DFT-s-OFDM system is given by a head $\mathbf{s}_h$ with length L_h, a tail $\mathbf{s}_t$ with length L_t, and the data $\mathbf{d}$ with length $N - L_h - L_t$. The role of the $\mathbf{s}_h$ sequence is to avoid a power regrowth of the data part in the last portion of the symbol due to the cyclicity of the IFFT operation, due to that, it can be used a very short sequence. The $\mathbf{s}_t$ role, in the presence of multipath propagation, is to generate to the next symbol the same energy leakage component that the symbol itself experiences at its beginning. So, the provided $\mathbf{s}_t$ is set to be longer than the delay spread of the channel. This emulates the cyclic property of the received signal as in traditional CP-based transmission: a necessary condition for enabling one-tap frequency domain equalization (BERARDINELLI *et al.*, 2016). These samples are concatenated forming $\mathbf{q}$ with size N, which is expressed as

$$\mathbf{q} = [\mathbf{s}_h \;\; \mathbf{d} \;\; \mathbf{s}_t]. \tag{1}$$

The sizes of L_h and L_t are tuned by taking into account the desired OOB emissions and the length of the impulse response of the fading channel. Here, since our focus is only on the INI reduction, the fading channel is not considered in our analysis.

Then, $\mathbf{q}$ passes through a normalized FFT $\mathbf{F}_N$ with size $N \times N$, which has its output $\mathbf{t}$ mapped to frequency subcarriers through a mapping scheme $\mathbf{M}$ with size $N_{\mathrm{FFT}} \times N$, generating $\mathbf{c}$ with length N_{FFT}. For the sake of simplicity and convenience, localized mapping is considered in our scenario, and $\eta = N/N_{\mathrm{FFT}}$.

The mapped signal $\mathbf{c}$ is processed by an IFFT $\mathbf{F}_{N_{\mathrm{FFT}}}^{-1}$ with size $N_{\mathrm{FFT}} \times N_{\mathrm{FFT}}$, resulting in $\mathbf{y}$, which is the transmitter output. Thus, the transmitted signal $\mathbf{y}$ with length N_{FFT} can be expressed as

$$\mathbf{y} = \mathbf{F}_{N_{\mathrm{FFT}}}^{-1} \mathbf{M} \mathbf{F}_N \, \mathbf{q}. \tag{2}$$

The receiver must act inversely with respect to the transmitter to obtain the data estimate. Therefore, its structure is composed of an FFT block, which has its output demapped into subcarriers that are processed by an IDFT. This sequence of steps results in the estimated signal composed of head, data, and tail. So, by discarding head and tail from the received signal, the estimated data is obtained. Thus, the receiver output $\hat{\mathbf{q}}$, without noise and channel fading, is given by

$$\hat{\mathbf{q}} = \mathbf{F}_N^{-1} \mathbf{M} \, \mathbf{F}_{N_{\mathrm{FFT}}} \, \mathbf{r}, \tag{3}$$

where $\mathbf{r}$ is the received signal. As the generalized DFT signal $\mathbf{q}$ is composed of head, data, and tail, it is necessary to discard the head and tail sequences in order to obtain the symbol estimate at the receiver $\hat{\mathbf{d}}$, which can be done as $\hat{\mathbf{d}} = \mathbf{q}[N_h : (N - N_t - 1)]$.

Figure 7 – Out-of-band emissions on CP-OFDM and G-DFT-s-OFDM.

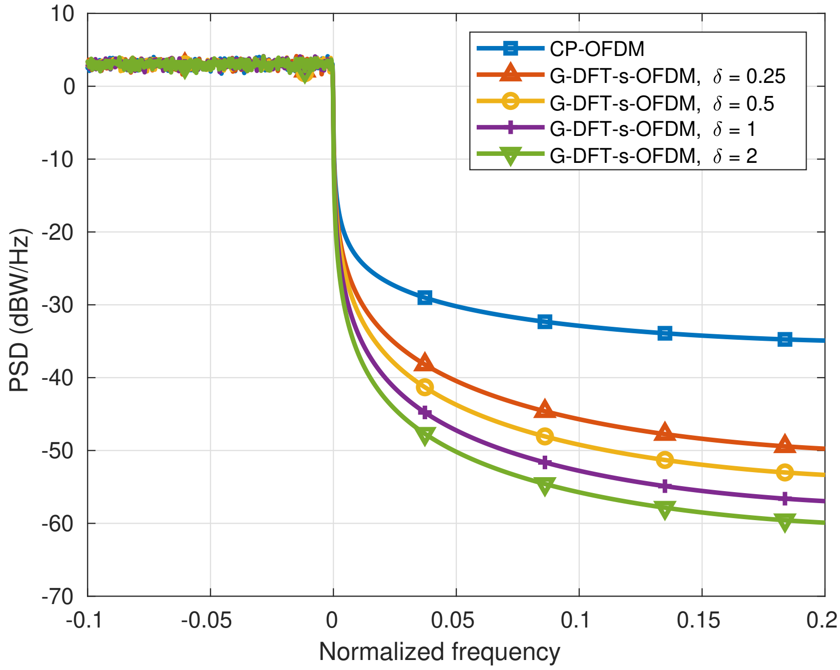

Source: Own authorship.

Figure 7 presents a power spectral density comparison between CP-OFDM and G-DFT-s-OFDM, detailing their out-of-band emissions, for $N = 2048$, $N_{FFT} = 4096$, $N_h = 16\delta$, $N_t = 80\delta$ and $\delta \in \{0.25, 0.5, 1, 2\}$. It is possible to see that by adopting G-DFT-s-OFDM the OOB emissions are reduced even with small values of N_h and N_t.

2.6 RELATED WORKS

Strategies to reduce INI have been studied by recent literature. Aiming to optimize network performance, the authors in (LOTFI; SEMIARI, 2021) derive a closed-form expression of the INI in a DFT-s-OFDM system, in order to allocate power to the subcarriers as well as the numerology of each endpoint. In (KIHERO *et al.*, 2019) a common CP for all numerologies is proposed, which minimizes the INI when compared with the standard individual CP used in 5G-NR. In (CHOI *et al.*, 2019) the OFDM transceiver is modified in order to use simple cyclic and frequency shift operations, designed to suppress the increase in the variance of the interference energy, by its turn reducing the INI effect. Furthermore, the authors in (ZHANG *et al.*, 2018) propose a INI cancellation scheme, which employs a window in order to attenuate the side lobes of the FFT symbols, *i.e.*, serving as a filter to the system. Then, an analytical expression for the INI power is derived, which is a function of the frequency response of the interfering subcarrier channel, the spectral distance and the overlap windows generated by the sender and receiver windows.

In addition, in (DEMIR; ARSLAN, 2020) the utilization of adaptive guards in time and frequency domains is shown as a solution to reduce the INI, along with a multi-window operation in the physical layer. An adaptive windowing operation is also used with a guard duration to reduce the unwanted emissions, together with a guard band to handle the INI level on the adjacent band. In (CEVIKGIBI *et al.*, 2022), a pre-equalization method is proposed to remove the INI that occurs in multiple numerology OFDM frame structures on the transmitter side. The INI level can be also used as a parameter to create a model, as presented in (CORREIA *et al.*, 2021), which can be used to build numerology profiles. As a consequence, one of the profiles can be adopted according to the current users/traffic pattern, enhancing the performance of the system. In summary, the schemes proposed by (LOTFI; SEMIARI, 2021; KIHERO *et al.*, 2019; CHOI *et al.*, 2019; ZHANG *et al.*, 2018; DEMIR; ARSLAN, 2020; CEVIKGIBI *et al.*, 2022) mainly deal with two approaches to handle the INI: filtering and different transmission strategies.

2.7 REMARKS

In this Section, the literature review for this work was presented. Taking into account the systems mentioned here, the system model used in this work to model the INI in 5G-NR networks using G-DFT-s-OFDM systems will be detailed in the next Section.

3 MATERIALS AND METHODS

In order to achieve the objectives specified in the proposal of this work, the feasibility of the G-DFT-s-OFDM for INI reduction in 5G-NR was studied. Initially, an algorithm was created to reproduce the conventional 5G-NR architecture. To model the multiple numerologies characteristic, it has a transmitter capable of simultaneously transmitting symbols of NSCS and WSCS numerologies, and a receiver able to extract those symbols from the received data. The algorithm was then enhanced to also support G-DFT-s-OFDM. This addition has changed the allocation of indexes (based on η) formerly made in the IFFT by the DFT.

3.1 SYSTEM MODEL

The organization of the 5G-NR transmitter takes into account that different numerologies will be transmitted simultaneously. Thus, in order to allocate the subcarrier indices in the IFFT in our example with two numerologies, a factor η is used as the subcarrier allocation ratio for the numerology with lower subcarrier spacing, while $1-\eta$ is the ratio for the numerology with larger subcarrier spacing. Figure 3 illustrates the difference between the NSCS and WSCS IFFT blocks in a scenario with $Q = 2$. For the scenario considered in this work, the first ηN subcarriers transmit data in the NSCS system, while the other ones are set to zero. On the other hand, the last $(1-\eta)N/Q$ subcarriers of the WSCS system transmit data, while the first $\eta N/Q$ ones are set to zero.

The CP in 5G-NR is generated by copying the last values of each symbol, and adding them at the beginning of symbol. This addition causes a displacement of the symbol position, which is responsible for breaking the orthogonality between the multiple numerologies as discussed in (NEMATI; ARSLAN, 2017) and shown in Figure 9.

Figure 8 – IFFT inputs on WSCS and NSCS numerologies.

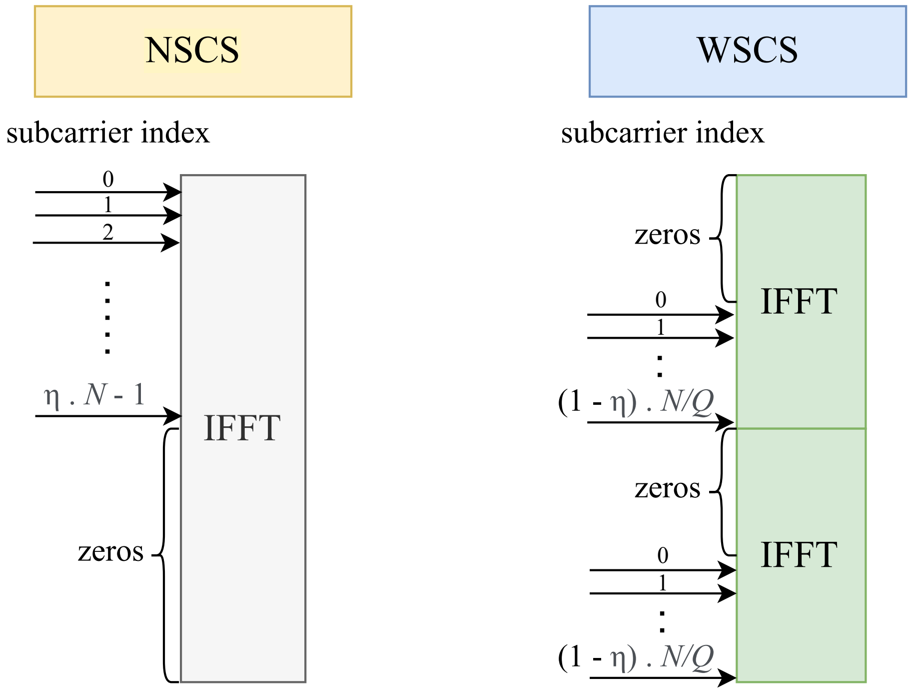

Source: Own authorship.

Figure 9 – Symbol organization for CP-OFDM with multiple numerologies.

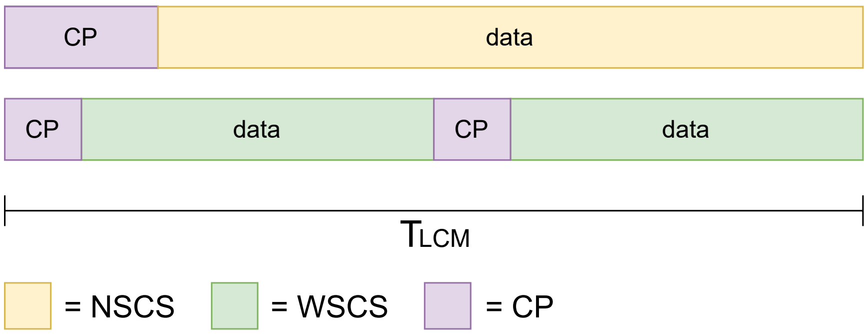

Source: Own authorship.

Figure 9 shows the symbol organization for CP-OFDM in the least common multiplier symbol duration (T_{LCM}) and evidences the CP length difference for NSCS and WSCS numerologies, which leads to symbol misalignment. For this image, $Q = 2$ - thus, it is possible to observe that two WSCS symbols are being transmitted for each NSCS symbol. Therefore, for higher values of Q the number of repetition of "CP + data"blocks for WSCS channels respects the Q's ratio.

Figure 10 shows side-by-side symbols from the CP-OFDM scheme and from the G-DFT-s-OFDM one for different numerologies, with $Q = 2$. The main differences are related to the CP replacement by a head and a tail, and the "adaptive"data length for G-DFT-s-OFDM systems, since changing head and tail length values impacts directly in the length reserved to place the data.

Figure 10 – Symbol structure comparison for the considered systems.

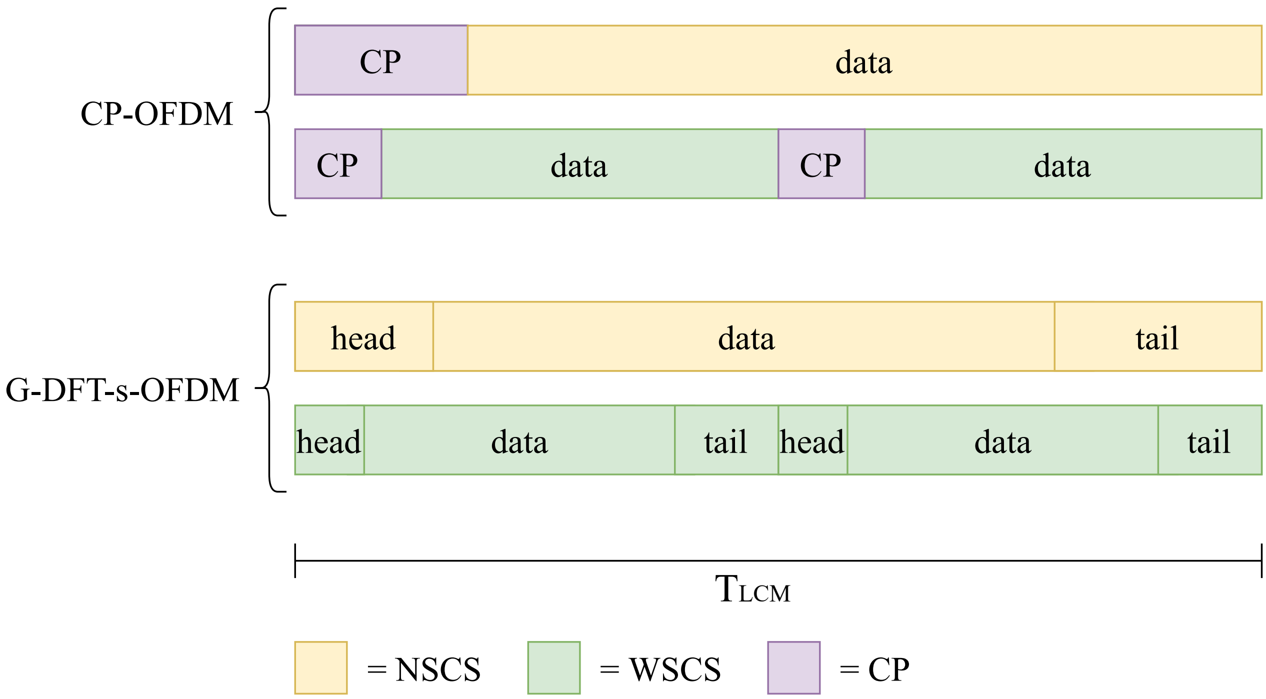

Source: Adapted from (BERARDINELLI, 2017)

Considering the scenario where G-DFT-s-OFDM symbols from an NSCS numerology $\mathbf{y}_n$, with length N_n, are transmitted together with Q G-DFT-s-OFDM symbols from a WSCS numerology $\mathbf{y}_w$, the overall transmitted signal $\mathbf{y}_o$ is

$$\mathbf{y}_o = \mathbf{y}_n + \mathbf{y}_w, \tag{4}$$

where $\mathbf{y}_w = [\mathbf{y}_{w,1} \ \dots \ \mathbf{y}_{w,Q}]$ and $\mathbf{y}_{w,i}$ is the i-th WSCS symbol, with length $N_w = N_n/Q$. At the NSCS receiver, and considering a scenario without both noise and fading channel, the N_n-length signal $\mathbf{r}_n$ for the NSCS case is given by

$$\mathbf{r}_n = \mathbf{y}_n + \mathbf{y}_{\text{INI},w}, \tag{5}$$

where $\mathbf{y}_n$ is the desired signal and $\mathbf{y}_{\text{INI},w}$ is the INI caused by the WSCS symbols, both with length N_n. Likewise, $\mathbf{y}_{\text{INI},w}$ can be expressed as

$$\mathbf{y}_{\text{INI},w} = \mathbf{F}_{N_n}\mathbf{c}_w, \tag{6}$$

where $\mathbf{c}_w$ is the mapped signal from the WSCS transmitter. This mismatch between the FFT size employed at the NSCS receiver and the WSCS symbols generated by a transmitter employing a different FFT size is what causes the INI.

On the other hand, for the WSCS case the N_w-length signal $\mathbf{r}_{w,i}$ for the i-th symbol can be expressed as

$$\mathbf{r}_{w,i} = \mathbf{y}_{w,i} + \mathbf{y}_{\text{INI},n}, \tag{7}$$

where $\mathbf{y}_{w,i}$ is the desired WSCS signal and $\mathbf{y}_{\text{INI},n}$ is the domain INI caused by the NSCS signal, both with length N_w. In addition, $\mathbf{y}_{\text{INI},n}$ is given by

$$\mathbf{y}_{\text{INI},n} = \mathbf{F}_{N_w}\mathbf{c}'_n, \tag{8}$$

where $\mathbf{c}'_n$ is the vector corresponding to the samples of the mapped NSCS signal $\mathbf{c}_n$ that fall into the N_w length window of the WSCS receiver. Again, the mismatch between the FFT size employed at the WSCS receiver and the NSCS symbol generated by a transmitter employing a different FFT size is what causes the INI.

3.2 REMARKS

The system model and the methodology considered in this work were detailed in this Section. Next, simulation results using the proposed model are shown and discussed.

4 RESULTS AND DISCUSSIONS

With the aim of evaluating the INI reduction performance of the G-DFT-s-OFDM with respect to the regular CP-OFDM systems, a simulation model was developed. Transmitted data was drawn from BPSK modulated symbols with unit power. In addition, $Q \in \{2, 4, 8\}$ was considered and the base numerology (with $\Delta_{\mu_0} = 15$ kHz) is always the NSCS for the sake of simplicity, since the ratio between the subcarrier spacings from different numerologies is the determinant factor in INI (DEMMER *et al.*, 2018). The base head length is $L_h = 16$ subcarriers, whereas the base tail length is $L_t = 80$ subcarriers. ZT G-DFT-s-OFDM was considered without loss of generality, since its OOB emissions are the same as the ones from UW G-DFT-s-OFDM (BERARDINELLI, 2017). The total number of subcarriers is $N = 2048$ for the lower numerology scenario, and only two simultaneous numerologies are considered, denoted by NSCS and WSCS, where $\eta = 0.5$. For the CP-OFDM system, the CP length is obtained by the sum of head and tail, since these lengths were fixed with the base values for the systems comparison, so that $L_{\text{CP}} = 96$. Additionally, only one RB per symbol was activated in order to analyze the impact of its INI in the entire system.

4.1 G-DFT-S-OFDM AGAINST CP-OFDM

The following results present the proposed system (G-DFT-s-OFDM) against the CP-OFDM. Since the G-DFT-s-OFDM does not use the cyclic prefix in its implementation, it is expected that the discontinuities of the symbols will be smoothed out, thus reducing the interference in these places. Also, due to the better spectral efficiency of that waveform, the absolute INI will also be reduced.

Figure 11 – INI of the G-DFT-s-OFDM and CP-OFDM schemes on the NSCS numerology for $Q = 2$.

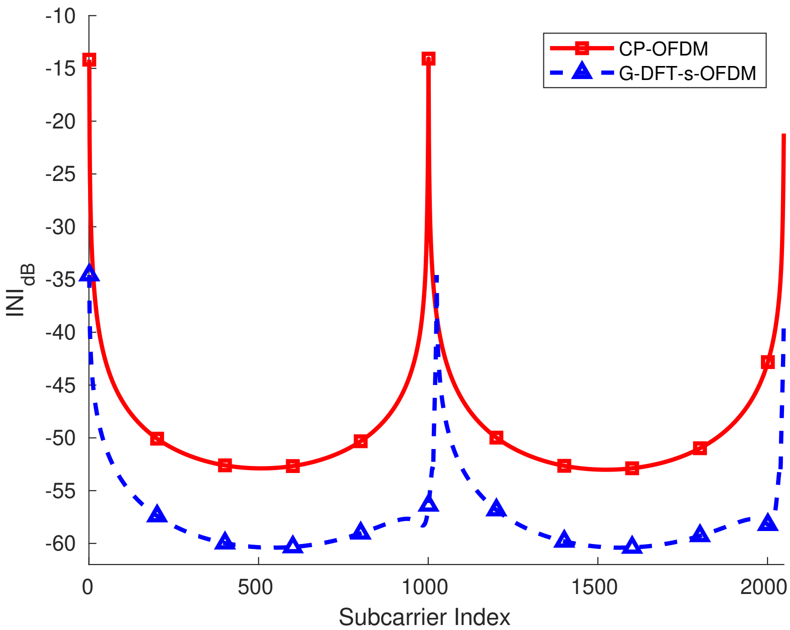

Source: Own authorship.

The INI experienced by the NSCS symbol for $Q = 2$ is illustrated in Figure 11. Due to the time misalignment between symbols the highest INI levels are observed at the symbol transition. In the CP-OFDM case, due to the CP length the symbol transition on WSCS happens before subcarrier 1024, which the is the middle subcarrier of this numerology for $\eta = 0.5$, $N = 2048$ and consequently $Q = 2$. This brings the INI peak about 15 subcarrier indexes to the left. In the G-DFT-s-OFDM system the alignment is not disturbed by the CP, making the peak of INI being observed at the middle of the NSCS symbol (subcarrier number 1024). More importantly, we observe that the INI peak with G-DFT-s-OFDM at this transition is at approximately -35 dB, which is 20 dB lower than that obtained in the CP-OFDM case.

Figure 12 presents the INI experienced by the Q symbols from the WSCS numerology and $Q = 2$. In the CP-OFDM case, the first symbol experiences the same INI as the one from G-DFT-s-OFDM systems, due to the position of the interfering RB on the NSCS system affecting only the second symbol from the WSCS system. However, in the case of G-DFT-s-OFDM the INI peak for the WSCS numerology at the symbol transition is at approximately -37 dB, which is 25 dB lower when compared to the CP-OFDM system.

In order to compare the performance of CP-OFDM and G-DFT-s-OFDM systems regarding the INI decay at the neighbor subcarriers of each numerology, the number of guard band subcarriers to reach INI levels of -40 and -50 dB was chosen as a benchmark. Table 2

Figure 12 – INI of the G-DFT-s-OFDM and CP-OFDM schemes on the WSCS numerology for $Q = 2$.

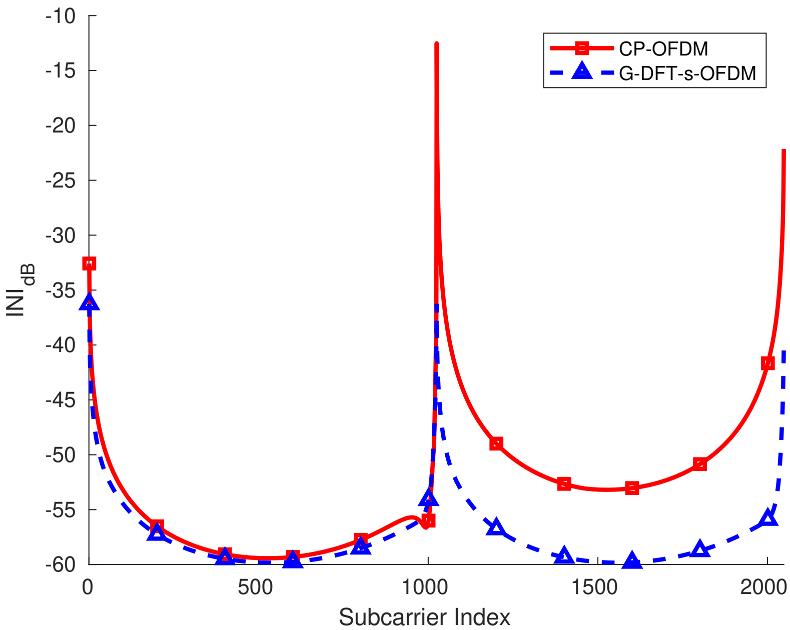

Source: Own authorship.

compares the guard band required for CP-OFDM and G-DFT-s-OFDM according to the type of numerology (NSCS or WSCS). We observe that the G-DFT-s-OFDM system requires a much smaller number of subcarriers to achieve the same INI level of CP-OFDM, evidencing that the use of G-DFT-s-OFDM is beneficial for 5G-NR networks in terms of spectral efficiency. As an example, to obtain $\text{INI} = -40$ dB for NSCS in this scenario, a guard band of 420 kHz is needed in CP-OFDM systems, whereas a guard band of only 30 kHz is needed for G-DFT-s-OFDM. If the INI threshold is of -50 dB, a guard band of almost 3 MHz is needed in CP-OFDM systems, whereas a guard band of only 135 kHz (22 times smaller) is needed for G-DFT-s-OFDM.

Table 2 – Number of subcarriers needed to reach a given level of INI for $Q = 2$.

Numerology	Scheme	$\text{INI} = -40$ dB	$\text{INI} = -50$dB
NSCS	CP-OFDM	28	199
	G-DFT-s-OFDM	2	9
WSCS	CP-OFDM	36	210
	G-DFT-s-OFDM	1	11

Source: Own authorship.

As seen before, the highest INI values happen at the symbols transitions. Thus, Table 3 presents a comparison between the maximum value of INI peaks found in the symbols transition for higher values of Q, 4 and 8. It can be seen that by employing G-DFT-s-OFDM we can reduce this INI by at least 8.9 dB in the worst case.

Higher values of Q are relevant scenarios due to their usability in real world conditions,

Table 3 – INI (in dB) found in symbol transitions for $Q = 4$ and 8.

Numerology	Scheme	Q = 4	Q = 8
NSCS	CP-OFDM	-14.03	-13.95
	G-DFT-s-OFDM	-27.25	-22.77
WSCS	CP-OFDM	-14.23	-13.94
	G-DFT-s-OFDM	-26.91	-23.16

Source: Own authorship.

allowing higher order numerologies to coexist closely with ones containing smaller subcarrier spacings.

Figure 13 – INI on the edge subcarriers for WSCS numerology for $Q \in \{2,4,8\}$.

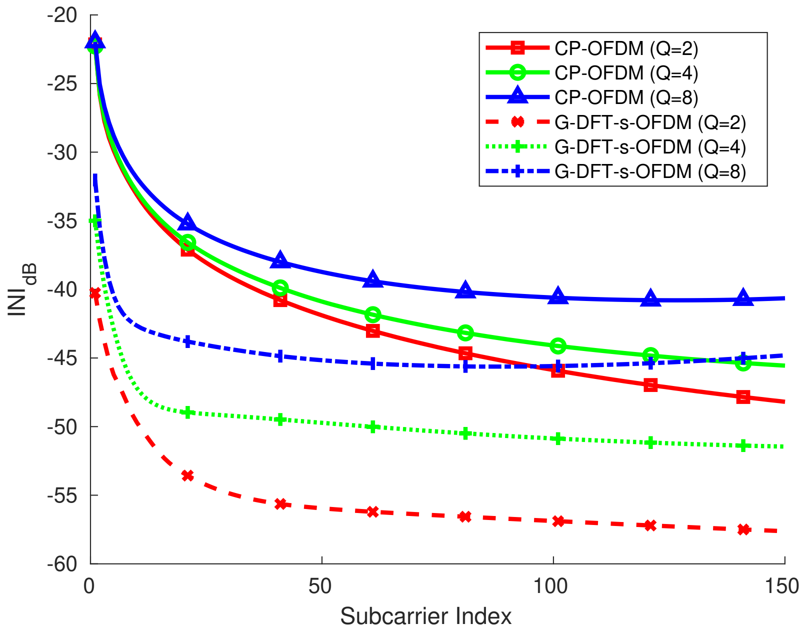

Source: Own authorship.

Figures 13 and 14 show the INI for WSCS and NSCS signals, respectively, with $Q \in \{2, 4, 8\}$ for both G-DFT-s-OFDM and CP-OFDM schemes. As we observe, when Q is high the INI peaks of the G-DFT-s-OFDM systems are also lower than that of the CP-OFDM, for both WSCS and NSCS numerologies, with a reduction of approximately 13 dB for $Q = 4$ and 9 dB for $Q = 8$ when using G-DFT-s-OFDM instead of CP-OFDM.

Figure 14 – INI on the edge subcarriers for NSCS numerology for $Q \in \{2,4,8\}$.

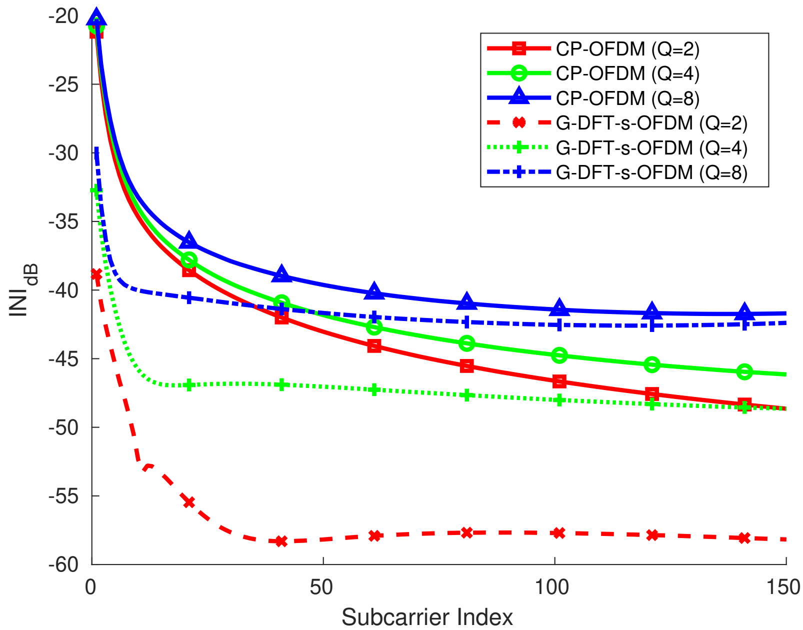

Finally, Table 4 compares G-DFT-s-OFDM and CP-OFDM in terms of the number of subcarriers needed to obtain a level of $\text{INI} = -40$ dB, with $Q = 4$ and $Q = 8$. G-DFT-s-OFDM requires a much smaller guard band to achieve the same INI level of CP-OFDM. For instance, with $Q = 4$, the guard band of G-DFT-s-OFDM is approximately 1.74 MHz smaller than that of CP-OFDM in NSCS, with the difference being of 1.32 MHz in WSCS. Such gap increases respectively to 5.64 and 3.72 MHz with $Q = 8$.

Table 4 – Number of subcarriers needed to reach $\text{INI} = -40$ dB with $Q = 4$ and 8.

Numerology	Scheme	$Q = 4$	$Q = 8$
NSCS	CP-OFDM	34	57
	G-DFT-s-OFDM	5	10
WSCS	CP-OFDM	27	43
	G-DFT-s-OFDM	5	12

Source: Own authorship.

4.2 HEAD AND TAIL SIZE VARIATION

Using different head and tail lengths in G-DFT-s-OFDM system allows the understanding of how that variation can affect the INI performance of the channels. Also, it helps to indicates the guard band amount that can be used to increase the data rate without loss of reliability and efficiency. The base head and tail lengths were multiplied by $\delta \in \{0.25, 0.5, 1, 2\}$.

The figures were generated for each Q and WSCS/NSCS numerologies in order to better display the results.

Again choosing -40 dB of INI as a benchmark level, the results presented in Figures 15, 16, 17, 18, 20 for, respectively, $Q = 2$ and $Q = 4$ considering both NSCS and WSCS numerologies and $Q = 8$ for the WSCS scenario reach this value on similar subcarrier indexes, showing that a reduced head/tail size can be used for different values of Q without impacting the required guard band size. For the NSCS scenario with $Q = 8$ presented in Figure 19, the -40 dB INI level requires a larger guard band when reducing the head/tail size. However, this is not the case for -37 dB of INI - the guard band required for this value is the same for all considered head/tail lengths in this scenario.

Figure 15 – Head and tail variation for NSCS numerology using $Q = 2$.

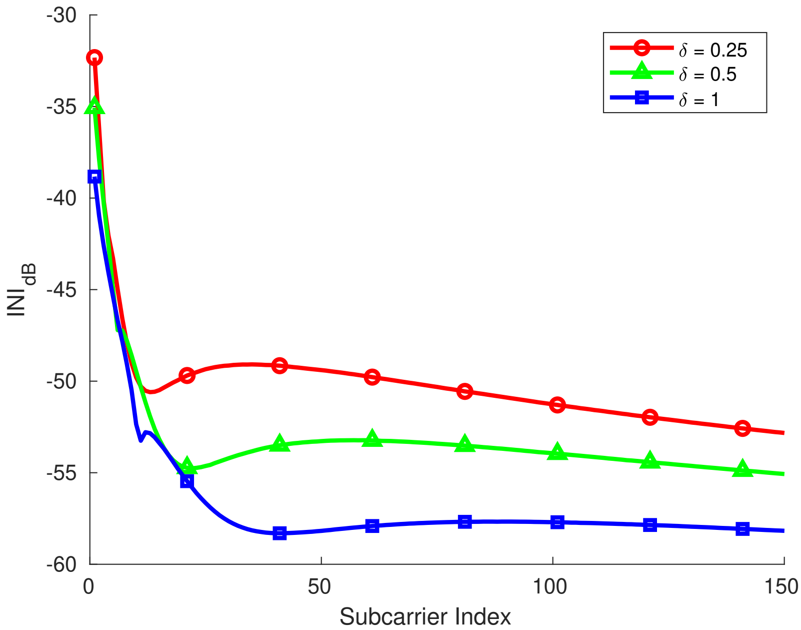

Figure 16 – Head and tail variation for WSCS numerology using $Q = 2$.

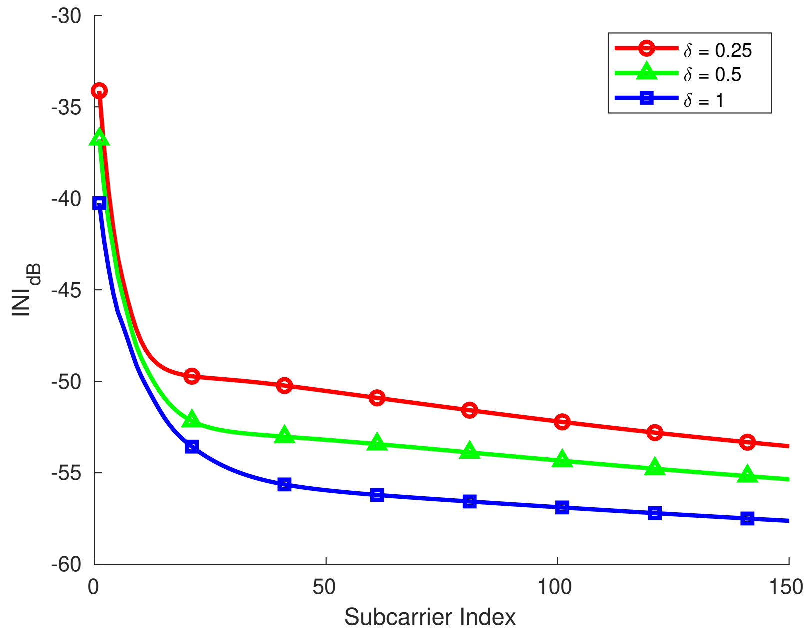

Figure 17 – Head and tail variation for NSCS numerology using $Q = 4$.

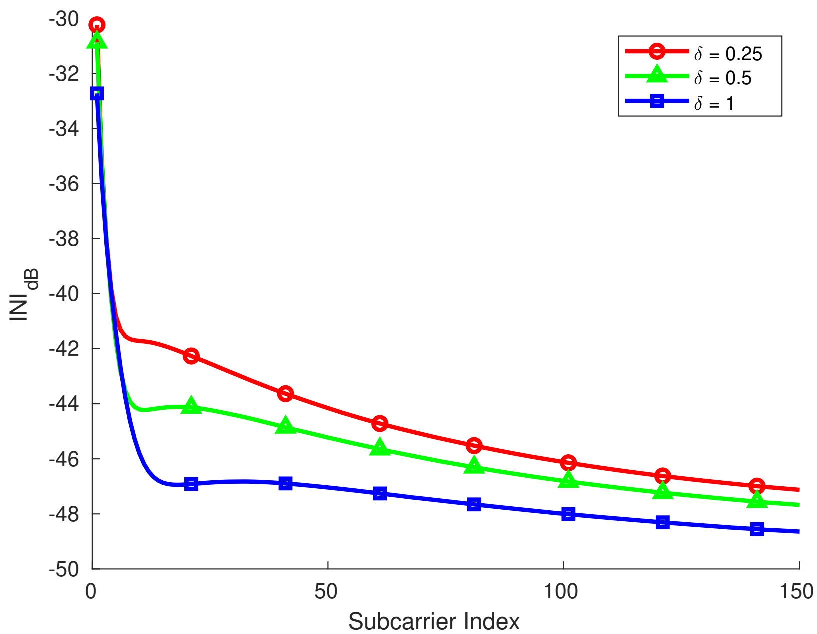

Figure 18 – Head and tail variation for WSCS numerology using $Q = 4$.

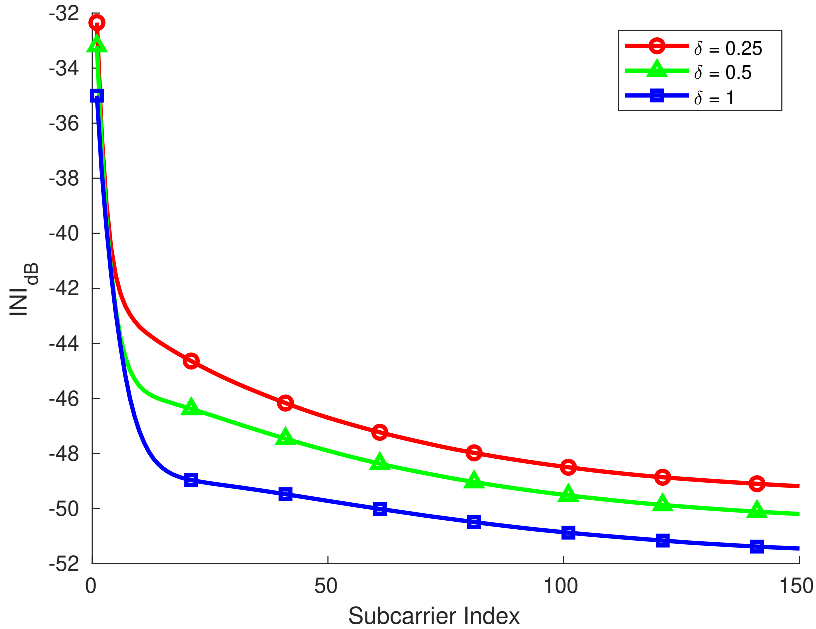

Figure 19 – Head and tail variation for NSCS numerology using $Q = 8$.

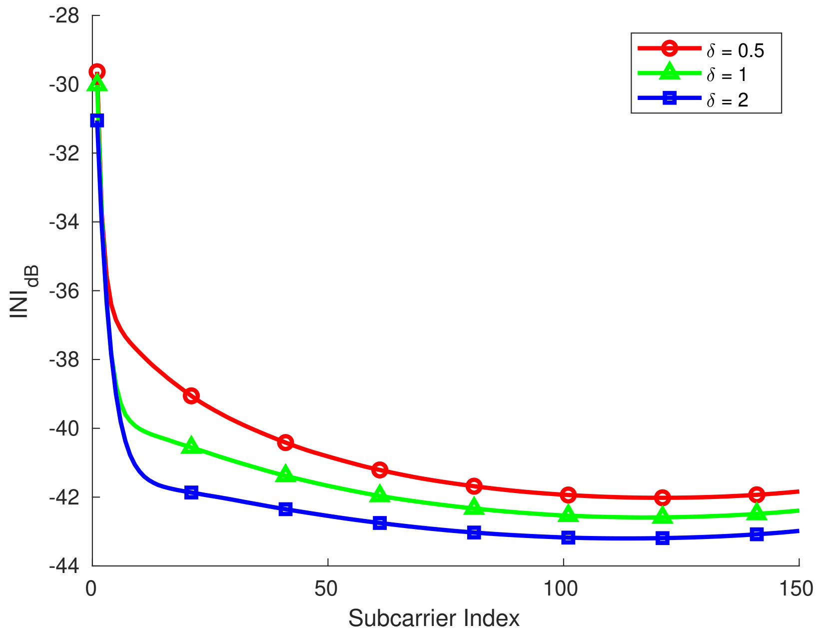

Figure 20 – Head and tail variation for WSCS numerology using $Q = 8$.

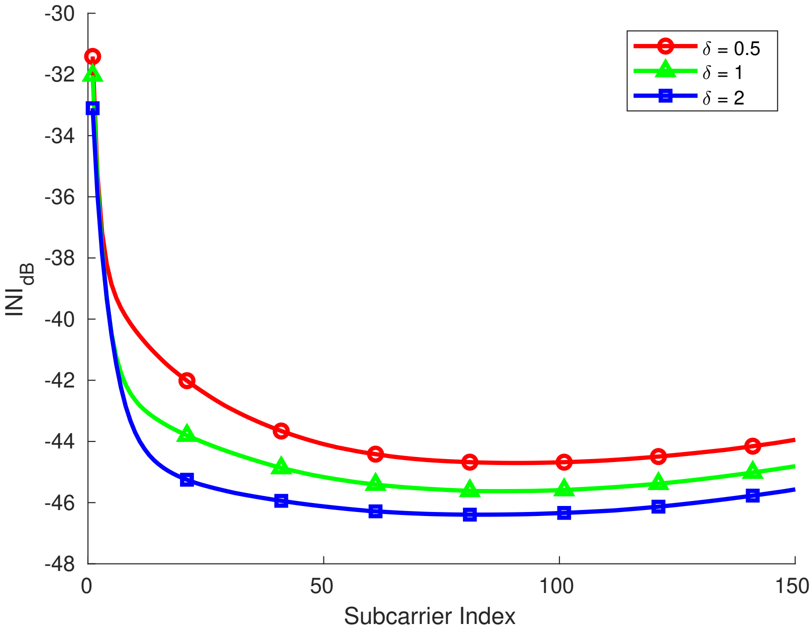

5 CONCLUSION

In this work, we have presented G-DFT-s-OFDM as an alternative waveform to reduce INI on 5G-NR networks. 5G-NR mobile networks standard were developed with CP-OFDM as their base waveform, with DFT-s-OFDM as an alternative in PAPR limited scenarios. The replacement of the CP by a flexible head and tail that fit the symbols' duration is a compatible new way which is shown to greatly reduce the INI observed in 5G-NR systems and improve their spectral efficiency, by requiring smaller guard bands to maintain a given INI level.

A thorough investigation was made through simulation considering a variation of the relevant parameters, such as the subcarrier spacing ration between numerologies Q, G-DFT-s-OFDM head and tail sizes. The analyzed scenarios take into account only one resource block per WSCS symbol, and its positioning being mirrored to the NSCS symbol in order to present how this RB impacts the signal transmitted in every numerology, making it possible to calculate the INI values. The variation of the considered Q helps to understand how the G-DFT-s-OFDM behaves in a situation closer to what occurs in the real world.

The G-DFT-s-OFDM waveform reduces the INI in the system, since it has better time and frequency localization, and better spectral efficiency. All the obtained results present a better INI performance for the G-DFT-s-OFDM system when compared with the standard waveform in 5G-NR. It is important to reiterate that the implementation complexity of this system is relatively low and its integration with the 5G-NR network is simple, since it is compatible with the CP-OFDM system and does not require extra filtering.

5.1 FUTURE WORKS

As future extensions to the present work we intend to use more complex interference cancellation schemes in order to further reduce the INI, such as the successive interference cancellation scheme, as well as extend it to multiple antenna systems. Also, the usage of a known interference between transmitter and receiver, in order to eliminate that in the receiver can assist in the interference impact quantization.

Other suggestions are a theoretical derivation of the INI obtained with G-DFT-s-OFDM systems and a comparison with filtered systems such as the DFT precoded filterbank one (JUNIOR *et al.*, 2021). The theoretical derivation can be used to validate the proposed system and leads to further insights, while the comparison with a filtered system can be interesting to see whether the INI performance obtained by the proposed system is close to the one from a filtered one. Finally, the system model can be refined, taking into account the fading channel to explore the INI effect on the BER results.

REFERENCES

(3GPP) 3rd G. P. P. NR - Base Station (BS) radio transmission and reception (Release 15). *Technical Specification 38.104, ver 15.1.0*, april 2018.

(3GPP) 3rd G. P. P. NR - Physical channels and modulation (Release 15). *Technical Specification 38.211, ver 15.1.0*, april 2018.

ABDULLAH, Dakhaz Mustafa; AMEEN, Siddeeq Y. Enhanced Mobile Broadband (eMBB): A review. **Journal of Information Technology and Informatics**, v. 1, n. 1, p. 13–19, 2021.

ANDREEV, Denis. Overview of ITU-T activities on 5G/IMT-2020. **Int. Telecommun. Union**, 2017.

ASSOCIATION, 5G Infrastructure PPP *et al.* 5G Vision-The 5G Infrastructure Public Private Partnership: the next generation of communication networks and services. **White Paper, February**, 2015.

BERARDINELLI, Gilberto. Generalized DFT-s-OFDM waveforms without cyclic prefix. **IEEE Access**, IEEE, v. 6, p. 4677–4689, 2017.

BERARDINELLI, Gilberto; PEDERSEN, Klaus I; SORENSEN, Troels B; MOGENSEN, Preben. Generalized DFT-spread-OFDM as 5G waveform. **IEEE Communications Magazine**, IEEE, v. 54, n. 11, p. 99–105, 2016.

BEYME, S; LEUNG, C. Efficient computation of DFT of Zadoff-Chu sequences. **Electronics Letters**, IET, v. 45, n. 9, p. 461–463, 2009.

BOCKELMANN, Carsten; PRATAS, Nuno; NIKOPOUR, Hosein; AU, Kelvin; SVENSSON, Tommy; STEFANOVIC, Cedomir; POPOVSKI, Petar; DEKORSY, Armin. Massive Machine-Type Communications in 5G: Physical and MAC-layer solutions. **IEEE Communications Magazine**, IEEE, v. 54, n. 9, p. 59–65, 2016.

CEVIKGIBI, Bugra Alp; DEMIRTAS, Ali Murat; GIRICI, Tolga; ARSLAN, Huseyin. Inter-Numerology Interference Pre-Equalization for 5G Mixed-Numerology Communications. **arXiv preprint arXiv:2201.09228**, 2022.

CHOI, Jaeyoung; KIM, Beomju; LEE, Kwonjong; HONG, Daesik. A Transceiver Design for Spectrum Sharing in Mixed Numerology Environments. **IEEE Transactions on Wireless Communications**, IEEE, v. 18, n. 5, p. 2707–2721, 2019.

CORREIA, Noélia; AL-TAM, Faroq; RODRIGUEZ, Jonathan. Optimization of Mixed Numerology Profiles for 5G Wireless Communication Scenarios. **Sensors**, Multidisciplinary Digital Publishing Institute, v. 21, n. 4, p. 1494, 2021.

DEMIR, Ali Fatih; ARSLAN, Hüseyin. Inter-numerology interference management with adaptive guards: A cross-layer approach. **IEEE Access**, IEEE, v. 8, p. 30378–30386, 2020.

DEMMER, David; GERZAGUET, Robin; DORE, Jean-Baptiste; RUYET, Didier Le. Analytical study of 5G NR eMBB co-existence. *In*: **2018 25th International Conference on Telecommunications (ICT)**. *[S.l.: s.n.]*, 2018. p. 186–190.

DOGAN-TUSHA, Seda; TUSHA, Armed; BASAR, Ertugrul; ALTHUNIBAT, Saud; QARAQE, Khalid; ARSLAN, Hüseyin. Inter-Numerology Interference in OFDM-IM Systems. **IET Communications**, Wiley Online Library, v. 15, n. 15, p. 1941–1949, 2021.

GSA. **LTE to 5G: March 2021 Global update**. 2021. Available at: https://gsacom.com/paper/lte-to-5g-march-2021-global-update/?utm=reports4g.

IBRAHIM, Mohamed makram jaffer; YOUSIF, Mohammed Jalal Aldeen Hassan; YOUSSEF, Mahmoud Zine El Abidine Mahmoud. **Power optimization in 5G network**. 2022. Phd Thesis (PhD Thesis), 2022.

JAWHAR, Yasir Amer; AUDAH, Lukman; TAHER, Montadar Abas; RAMLI, Khairun Nidzam; SHAH, Nor Shahida Mohd; MUSA, Mustafa; AHMED, Mustafa Sami. A review of partial transmit sequence for PAPR reduction in the OFDM systems. **IEEE Access**, IEEE, v. 7, p. 18021–18041, 2019.

JUNIOR, Rogério Pereira; ROCHA, Carlos A. F. da; CHANG, Bruno S.; RUYET, Didier Le. A novel DFT precoded filter bank system with iterative equalization. **IEEE Wireless Communications Letters**, v. 10, n. 3, p. 478–482, 2021.

KAKKAVAS, Anastasios; XU, Wen; LUO, Jian; CASTANEDA, Mario; NOSSEK, Josef A. On PAPR characteristics of DFT-s-OFDM with geometric and probabilistic constellation shaping. *In*: IEEE. **2017 IEEE 18th International Workshop on Signal Processing Advances in Wireless Communications (SPAWC)**. *[S.l.]*, 2017. p. 1–5.

KIHERO, Abuu B; SOLAIJA, Muhammad Sohaib J; ARSLAN, Hüseyin. Inter-Numerology Interference for Beyond 5G. **IEEE Access**, IEEE, v. 7, p. 146512–146523, 2019.

KIM, Minhoe; LEE, Woongsup; CHO, Dong-Ho. A novel PAPR reduction scheme for OFDM system based on deep learning. **IEEE Communications Letters**, IEEE, v. 22, n. 3, p. 510–513, 2017.

LI, Zexian; UUSITALO, Mikko A; SHARIATMADARI, Hamidreza; SINGH, Bikramjit. 5G URLLC: Design challenges and system concepts. *In*: IEEE. **2018 15th international symposium on wireless communication systems (ISWCS)**. *[S.l.]*, 2018. p. 1–6.

LOTFI, Fatemeh; SEMIARI, Omid. Performance Analysis and Optimization of Uplink Cellular Networks with Flexible Frame Structure. *In*: IEEE. **2021 IEEE 93rd Vehicular Technology Conference (VTC2021-Spring)**. *[S.l.]*, 2021. p. 1–5.

MAKNI, Mariem; BAKLOUTI, Mouna; NIAR, Smail; BIGLARI-ABHARI, Morteza; ABID, Mohamed. Heterogeneous multi-core architecture for a 4G communication in high-speed railway. *In*: IEEE. **2015 10th International Design & Test Symposium (IDT)**. *[S.l.]*, 2015. p. 26–31.

MYUNG, Hyung G; LIM, Junsung; GOODMAN, David J. Single carrier FDMA for uplink wireless transmission. **IEEE vehicular technology magazine**, IEEE, v. 1, n. 3, p. 30–38, 2006.

NEMATI, Mahyar; ARSLAN, Hüseyin. Low ICI symbol boundary alignment for 5G numerology design. **IEEE Access**, IEEE, v. 6, p. 2356–2366, 2017.

OKOGBAA, Fred Chimzi; AHMED, Qasim Zeeshan; KHAN, Fahd Ahmed; ABBAS, Waqas Bin; CHE, Fuhu; ZAIDI, Syed Ali Raza; ALADE, Temitope. Design and Application of Intelligent Reflecting Surface (IRS) for Beyond 5G Wireless Networks: A Review. **Sensors**, MDPI, v. 22, n. 7, p. 2436, 2022.

OLIMID, Ruxandra F; NENCIONI, Gianfranco. 5G Network Slicing: A Security Overview. **IEEE Access**, IEEE, v. 8, p. 99999–100009, 2020.

TERRY, John; HEISKALA, Juha. **OFDM wireless LANs: A theoretical and practical guide**. *[S.l.]*: Sams publishing, 2002.

WEINSTEIN, Stephen B. The history of orthogonal frequency-division multiplexing [history of communications]. **IEEE Communications Magazine**, IEEE, v. 47, n. 11, p. 26–35, 2009.

WEISS, Timo A; JONDRAL, Friedrich K. Spectrum pooling: an innovative strategy for the enhancement of spectrum efficiency. **IEEE communications Magazine**, IEEE, v. 42, n. 4, p. 8–14, 2004.

WULICH, Dov. Definition of efficient PAPR in OFDM. **IEEE communications letters**, IEEE, v. 9, n. 9, p. 832–834, 2005.

WUNDER, Gerhard; FISCHER, Robert FH; BOCHE, Holger; LITSYN, Simon; NO, Jong-Seon. The PAPR problem in OFDM transmission: New directions for a long-lasting problem. **IEEE Signal Processing Magazine**, IEEE, v. 30, n. 6, p. 130–144, 2013.

ZHANG, Xiaoying; ZHANG, Lei; XIAO, Pei; MA, Dongtang; WEI, Jibo; XIN, Yu. Mixed Numerologies Interference Analysis and Inter-Numerology Interference Cancellation for Windowed OFDM Systems. **IEEE Transactions on Vehicular Technology**, IEEE, v. 67, n. 8, p. 7047–7061, 2018.